Received: 23 September 2020 | Revised: 23 November 2020 | Accepted: 29 November 2020

DOI: 10.1002/jbio.202000385

FULL ARTICLE

JOURNAL OF BIOPHOTONICS

A representation learning approach for recovering scatter-corrected spectra from Fourier-transform infrared spectra of tissue samples

Arne P. Raulf[1,2*] | **Joshua Butke**[1,2] | **Lukas Menzen**[1] | **Claus Küpper**[1,3] | **Frederik Großerueschkamp**[1,3] | **Klaus Gerwert**[1,3] | **Axel Mosig**[1,2*]

[1]Center for Protein Diagnostics, Ruhr-University Bochum, Gesundheitscampus 4, Bochum, Germany

[2]Bioinformatics Group, Department for Biology and Biotechnology, Ruhr-University Bochum, Gesundheitscampus 4, Bochum, Germany

[3]Chair of Biophysics, Department for Biology and Biotechnology, Ruhr-University Bochum, Gesundheitscampus 4, Bochum, Germany

***Correspondence**
Arne P. Raulf and Axel Mosig, Center for Protein Diagnostics, Ruhr-University Bochum, 44801 Bochum, Germany.
Email: arne.raulf@rub.de (A.P.R.)
axel.mosig@bph.rub.de (A.M.)

Funding information
Deutsche Forschungsgemeinschaft, Grant/Award Number: MO 2804/1-1

Abstract

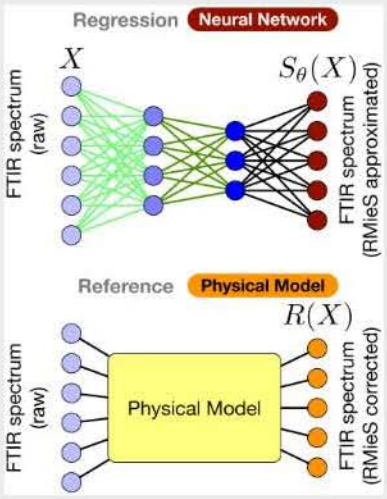

Infrared spectra obtained from cell or tissue specimen have commonly been observed to involve a significant degree of scattering effects, often Mie scattering, which probably overshadows biochemically relevant spectral information by a nonlinear, nonadditive spectral component in Fourier transform infrared (FTIR) spectroscopic measurements. Correspondingly, many successful machine learning approaches for FTIR spectra have relied on preprocessing procedures that computationally remove the scattering components from an infrared spectrum. We propose an approach to approximate this complex preprocessing function using deep neural networks. As we demonstrate, the resulting model is not just several orders of magnitudes faster, which is important for real-time clinical applications, but also generalizes strongly across different tissue types. Using Bayesian machine learning approaches, our approach unveils model uncertainty that coincides with a band shift in the amide I region that occurs when scattering is removed computationally based on an established physical model. Furthermore, our proposed method overcomes the trade-off between computation time and the corrected spectrum being biased towards an artificial reference spectrum.

Arne P. Raulf and Joshua Butke contributed equally to this study.

[Correction added on 11 January, after first online publication: Axel Mosig was designated as corresponding author]

KEYWORDS
deep neural network, Fourier-transform infrared microscopy, representation learning, resonant mie scattering

1 | INTRODUCTION

Fourier transform infrared (FTIR) spectroscopic imaging of biological samples provides pixel spectra at high spatial resolution which carry a highly informative fingerprint of the biochemical status of the sample. FTIR microscopy thus has been applied successfully in characterizing the disease state of tissue samples of different types from several different organs.[1–4] However, the raw spectra obtained from FTIR imaging experiments inherently suffer from scattering and the effect that Beer–Lambert's law is not applicable to such spectra, since the samples are heterogeneous.[5,6] Following the chemical information cannot be obtained from the measured spectra without correction. The most prominent scattering effect in FTIR imaging of biological samples is Mie scattering,[6–10] which affect the absorbance spectra and complicates the data analysis.[11]

This Mie scattering effect is observable when applying FTIR imaging to biological samples. Here, cells, nuclei or other cellular components within a certain size range[7,8] lead to a Mie scattering effect. This model led to the development of first correction procedures[12] based on the *extended multiplicative signal correction* algorithm.[13] This approach was extended by the authors of Reference 14, who introduced an iterative correction procedure for resonant Mie scattering (RMieS). While this approach takes into account scattering only, it has recently been further improved upon by approximating the complete Mie extinction through complex valued refractive indices of the scatterers.[15] In short, an FTIR pixel spectrum observed in an hyperspectral microscopic image can be a mixture of Mie scattering, non-linear effects, resonant absorption factors and other optical effects, which has led to the development of correspondingly complex computational correction procedures. None of these algorithms model yet the correct electromagnetic theory to obtain pure absorbance spectra but each is well suited for given applications.

In FTIR imaging on biological samples several studies have shown that Mie scattering correction solely can help to provide spectra sufficient for classification. Therefore, we will concentrate here on this well established procedure regardless of the justified discussion that there are other disturbing optical effects. While the very recent ME-EMSC approach[15] for Mie scattering correction promises great improvement over the less elaborate scattering model of the RMieS approach, our contribution is focused on the latter approach,[14] which has been popular in a large range of studies.[1,2,16] Throughout this manuscript, we will refer to the approach from Reference[14] as *RMieS correction*. This approach employs a reference spectrum, which represents an idealized baseline of a scattering-free infrared spectrum. This spectrum is used iteratively to approximate the measured, distorted spectra to a corrected spectrum for classification using the *extended multiplicative signal correction*[14]. Because of its iterative nature there is a strong trade-off of between time and accuracy to reach satisfactory results, making it computationally expensive.

Deep learning approaches have recently impacted the preprocessing and classification of infrared microscopic spectra.[17–19] Magnussen et al. introduced a convolutional neural network based autoencoder to recover absorbance spectra from scattered FTIR spectra.[20] Based on a deep convolutional neural network, the scattered input spectrum is transformed into a 22-dimensional latent space, from which inverse convolutions recover the pure absorbance spectrum. The network is trained on scattered input spectra against their ME-EMSC corrected absorbance spectra; based on a reference dataset of single fungal cell FTIR images, the absorbance spectra recovered from the neural network exhibit strong similarity to ME-EMSC corrected spectra across different growth conditions. In a similar direction, the authors in Reference[19] introduced an approach that employs a one-dimensional variant of the U-Net architecture[21] that approximates the removal of scattering resulting from poly(methyl methacrylate) (PMMA) spheres to recover "pure absorbance" spectra. As training data, the authors in Reference 19 use simulated scattering following a PMMA sphere specific model proposed in References 22 and 23.

In another recent contribution, we demonstrated that in the presence of sufficient data for training, deep neural networks may circumvent RMieS correction algorithm.[18] This approach is based on *representation learning*[24], specifically by employing the approach introduced in Reference 25 to perform unsupervised pre-training followed by supervised fine-tuning to classify pixel spectra into a discrete set of classes, that is, tissue components.

While the neural network introduced in Reference 18 involves training data obtained from RMieS corrected spectra and thus involves RMieS correction in an implicite manner, the model possesses no explicit knowledge of Mie scattering. Yet, it has been hypothesized in Reference 18 that, due to the strong generalization capability of the network, it may have learned to disentangle the raw spectra

into an abstract representation that separates scattering from the molecular spectrum. Our present contribution further investigates this hypothesis by explicitly training the network to approximate the complex function computed by the RMieS correction procedure. The rationale behind our present study is roughly as follows: We replace the final layer of a pretrained classifying neural network by a regression layer to learn RMieS correction–if supervised finetuning of the pretrained regression network successfully learns RMieS correction, this provides evidence about the disentanglement in the classifying network, namely that the pretraining helps to disentangle those variances that are due to resonant Mie scattering.

Bayesian approaches are a folklore approach to assess the statistical uncertainty of neural network classifications by considering the edge weights of a neural network as being sampled from a statistical process.[26,27] In the context of deep neural networks, Bayesian approaches have recently become particular relevant through dropout-learning, where neurons in specific layers are randomly deactivated.[28] This relatively simple idea has been coupled with Bayesian statistics in the seminal recent work by Gal et al.[29] which yields Bayesian uncertainties for output variables of neural networks that can be trained very efficiently using dropout learning. Applied to neural networks that approximate physical models, as investigated in our present contribution, this approach is highly attractive to estimate confidence of both the trained neural network and the underlying physical model.

In a broader context, deep neural networks were a major driver for recent progress in the analysis of microscopic image data. In fluorescence microscopy, for example, deep neural networks have been employed to compensate for spatial or temporal undersampling[30] or to enhance confocal microscopic images to superresolution imagery.[30,31] In another recent contribution, Ounkomol et al.[32] demonstrated the inference of fluorescence microscopic images from transmitted light micropscopy. A perspective emerging from these contributions is that deep neural networks have the ability to approximate physical processes behind different microscopic modalities, which has been an important ingredient for the rapid progress driven by deep neural networks in the analysis of biomedical images of both cellular[33] and tissue[34] samples.

2 | METHODS

embedded (FFPE) thin-sections of colon cancer associated tissue samples, sliced into 5 μm sections placed on LowE slides (Kevley Technologies, Chesterland, OH, USA). Infrared microscopic images were acquired using a Cary 620 infrared microscope by Agilent (Santa Clara, California, USA) in combination with a Cary 670 spectrometer in transflection mode and using a focal plane detector with 128 × 128 elements. The resulting raw spectra in the spectral range between 3700 and 950 cm^{-1} were preprocessed using the resonance-Mie correction procedure from Reference[35] applied to the spectral range from 2300 to 950 cm^{-1}. The samples were subdivided into one dataset $FFPE_{pt}$ for pretraining (see Section 3), and one dataset $FFPE_{ft}$ for supervised training (finetuning) the regression-model. The tissue microarray data from Reference 18 were used for training using an identical subdivision into training and validation data as described in Reference 18. Whole-slide images from Reference 2 were used as independent test sets.

3 | APPROACH

Our general approach is to extend the stacked autoencoder based network topology and training

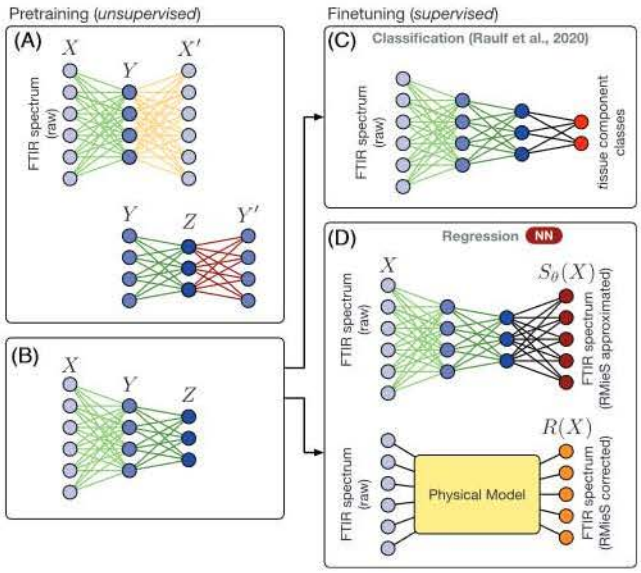

FIGURE 1 Overview of our approach to train a regression network (panel D) that approximates resonant Mie scattering (RMieS) correction based on unsupervised pretraining through stacked autoencoders (panels A and B). The approach is similar to the tissue component classifier proposed in Reference 18 (panel C).

processes behind different microscopic modalities, which has been an important ingredient for the rapid progress driven by deep neural networks in the analysis of biomedical images of both cellular[33] and tissue[34] samples.

2 | METHODS

2.1 | Dataset

For our study, we used datasets from References 2 and 18 that we briefly recapitulate for the sake of completeness. All samples were recruited from formalin fixed parrafin

FIGURE 1 Overview of our approach to train a regression network (panel D) that approximates resonant Mie scattering (RMieS) correction based on unsupervised pretraining through stacked autoencoders (panels A and B). The approach is similar to the tissue component classifier proposed in Reference 18 (panel C). Each output neuron of the regression network (indicated in dark red in panel D) learns regression of one specific wavenumber of the RMieS corrected spectrum, the regression loss is measured as the root-mean-squared error between the physical model $R(X)$ and the approximation $S_\theta(X)$ across all data points X

procedure from Reference 18 for classifying infrared pixel spectra to obtain a neural network that approximates the RMieS correction procedure from Reference 35 as illustrated in Figure 1. In fact, we used the RMieS correction implementation described in Reference 35 to produce training and validation data; to introduce some essential notation, we denote an RMieS corrected spectrum $y = R(x)$, where R denotes the RMieS correction procedure and x an uncorrected raw spectrum from one of the datasets.

Specifically, we use the paradigm of unsupervised pretraining as established in References 25 and 36, where an unsupervised pretraining on unlabeled data is used to give the initial mode for the used weight matrices in further training stages. While in Reference 18, these pretrained models underwent supervised finetuning to train a classifier network, this present contribution deals with a regression network aiming to approximate the RMieS correction function rather than aiming to classify pixel spectra. In other words, we deal with a neural network whose output layer represents Mie-corrected infrared spectra. To this end, we replace the transfer function of the output layer from a softmax function commonly used for classifying networks to a linear activation function suiting the requirements of a regression model. All regression models are based on an unsupervised Contractive Stacked Autoencoder[25] which was trained only on

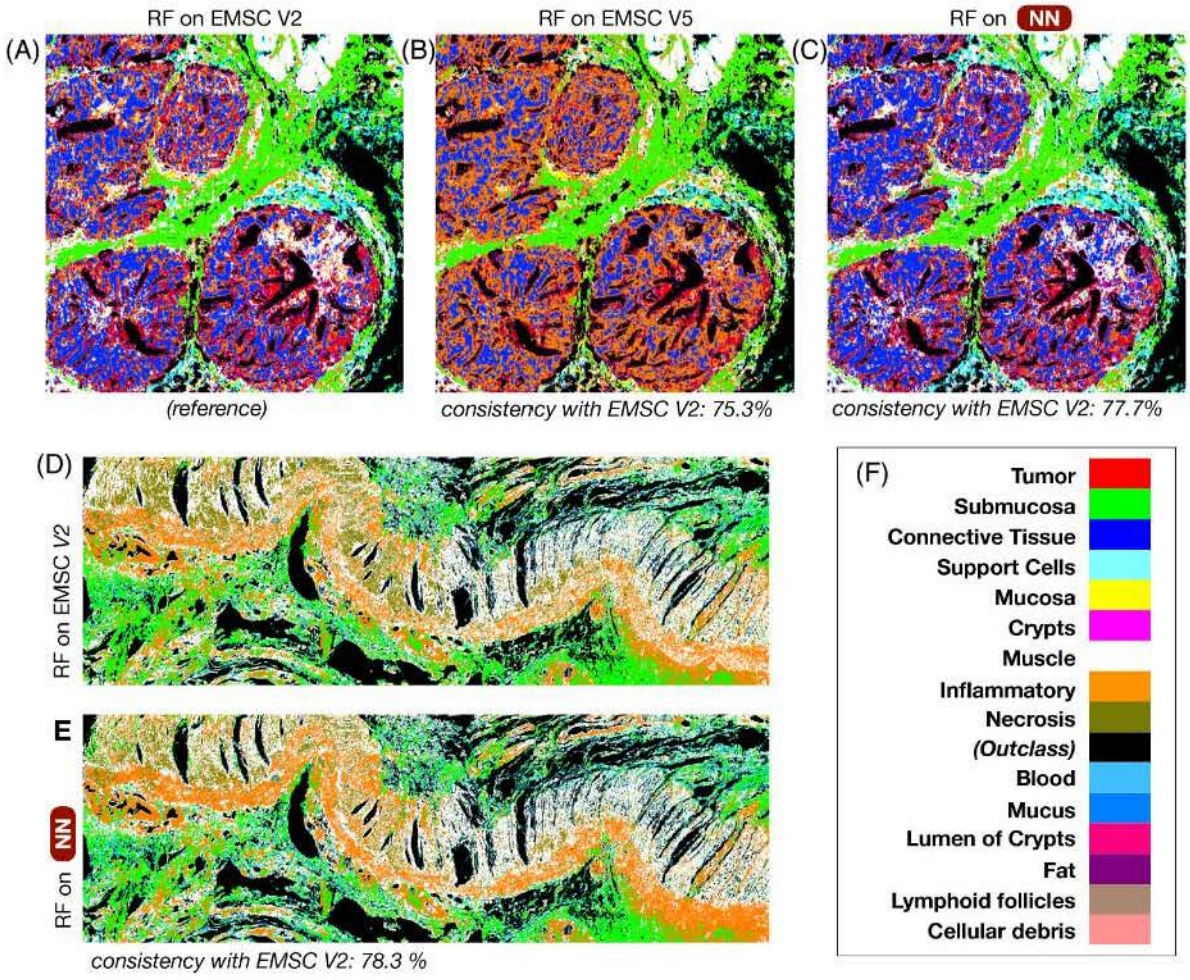

FIGURE 2 Panel A displays classification results of the random forest classifier from Reference 1 applied to the Fourier transform infrared (FTIR) spectra corrected with the *EMSC V2* implementation of the resonant Mie scattering (RMieS) correction. Panel B displays classification results obtained from the same classifier, but spectra corrected using the *EMSC V5* implementation of the FTIR spectra.[2] Panel C displays spectra corrected by the regression network S_θ that was trained to approximate the correction as implemented in *EMSC V2*. The consistency of different preprocessing approaches was computed as an accuracy of panels B (.753) and C (.777) using panel A as ground truth. Panels D and E display classification results of the random forest classifier from Reference 1, once applied to the FTIR spectra corrected with the *EMSC V2* implementation of the RMieS correction of a large whole-slide image (panel D) and once applied to the spectra corected using the apporximation through neural network S_θ (panel E). The index color map of the class labels obtained from the random forest classifier is displayed in panel F

the $FFPE_{pt}$ dataset. Throughout the paper, we will use θ to denote the parameters obtained from supervised finetuning, and $y = S_\theta(x)$ the network with parameters θ applied to input spectrum x, that is, the approximation of the corrected spectrum of x. During training, we used root mean square error as loss function.

3.1 | Validation measures

We validate our trained model θ on each of the validation datasets F at three levels. At the first level, we investigate the root mean square error $RMSE_\theta = \sum_{x \in F} \| R(x) - S_\theta(x) \|$. On a second level of validation, we used an existing random forest based classifier C from a previous study[1] that classifies a Mie corrected spectrum y into one out of nineteen different tissue component classes $C(y)$, and compared the output classes of the ground truth $C(R(x))$ with the classification obtained from an approximated correction, that is, $C(S_\theta(X))$. We will refer to the classifier C as a *downstream* model and thus refer to this validation approach as *downstream validation*.

On a third level of validation, we assess uncertainty of the trained regression model based on the Bayesian dropout approach proposed by Gal et al[29], which systematically integrates the concept of *dropout layers* (ie, the randomized dropping of neurons in specific layers) into an approximation of a Gaussian process. The statistical processes can be introduced into trained neural networks by using the usual dropout[28] not only as a tool to prevent overfitting on the training dataset but also during the test phase to randomly exclude 50% of neurons at test time. By excluding neurons at test time, one obtains a Bernoulli distribution over all different models of the trained network, which approximates the variational inference and finally approximates the deep Gaussian process. The latter step yields a tool to interpret deep neural networks as models by considering the prediction itself, the mean of the prediction and the variance of this process.

The RMieS correction procedure is also highly time sensitive, which led us to validate the running time difference between the RMieS correction reference implentation and its neural network approximator. As an iterative approach that needs to be applied to each individual pixel spectrum in an infrared microscopic image, practical running times can amount to hours when dealing with whole slide images that comprise tens of millions of pixel spectra,[2] where several iterations of the RMieS correction procedure may be required to achieve high quality corrected spectra. At the same time, it is not straightforward to implement the RMieS correction algorithm in a way that the parallelization capability of graphics hardware can be fully exploited.[35] Here, the potential promise of an approximator network is a large increase in processing speed, since common neural network frameworks can inherently and fully exploit parallelization capability. For the sake of comparability, graphics processing units were used only for training

TABLE 1 Running times obtained from RMieS correction reference implementation (EMSC) and the approximation by neural network (NN) for a dataset size of 360 000 spectra

Model	EMSC	NN

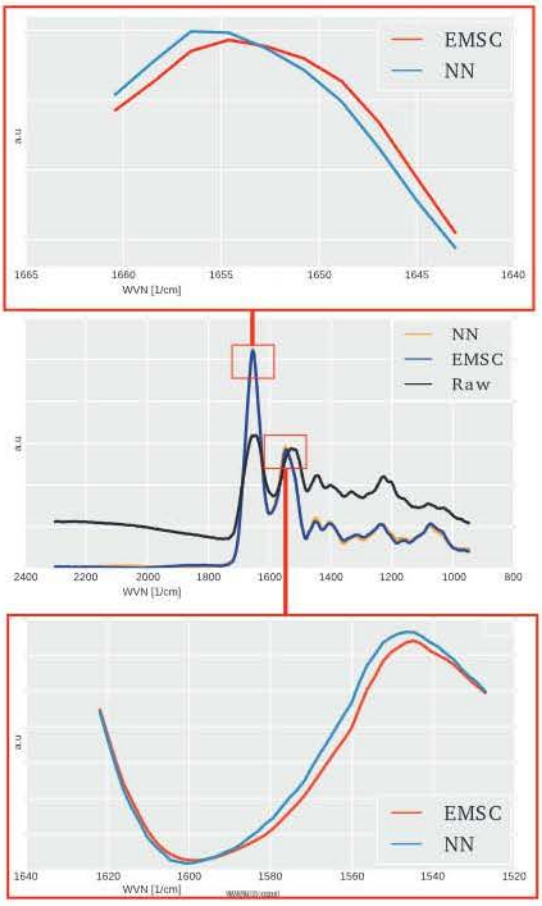

FIGURE 3 Middle: Example of an Fourier transform infrared (FTIR) spectrum from formalin fixed parrafin embedded (FFPE) tissue, shown as raw spectrum (black), corrected by the resonant Mie scattering (RMieS) correction algorithm from Reference 14

The RMieS correction procedure is also highly time sensitive, which led us to validate the running time difference between the RMieS correction reference

TABLE 1 Running times obtained from RMieS correction reference implementation (EMSC) and the approximation by neural network (NN) for a dataset size of 360 000 spectra

Model	EMSC	NN
Time for val.-set	64.99 sec	10.65 sec
Time per spectrum	118.23 μsec	28.96 μsec

Note: Recorded times were averaged over 10 runs each.
Abbreviation: RMieS, resonant Mie scattering.

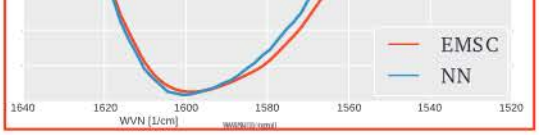

FIGURE 3 Middle: Example of an Fourier transform infrared (FTIR) spectrum from formalin fixed parrafin embedded (FFPE) tissue, shown as raw spectrum (black), corrected by the resonant Mie scattering (RMieS) correction algorithm from Reference 14 (blue) and corrected by the neural network S_θ that approximates the RMieS correction. Both the amide I (top) and amide II (bottom) peak exhibit a band shift when comparing to the reference implementation of RMieS correction (EMSC V2) and the approximating neural network (NN)

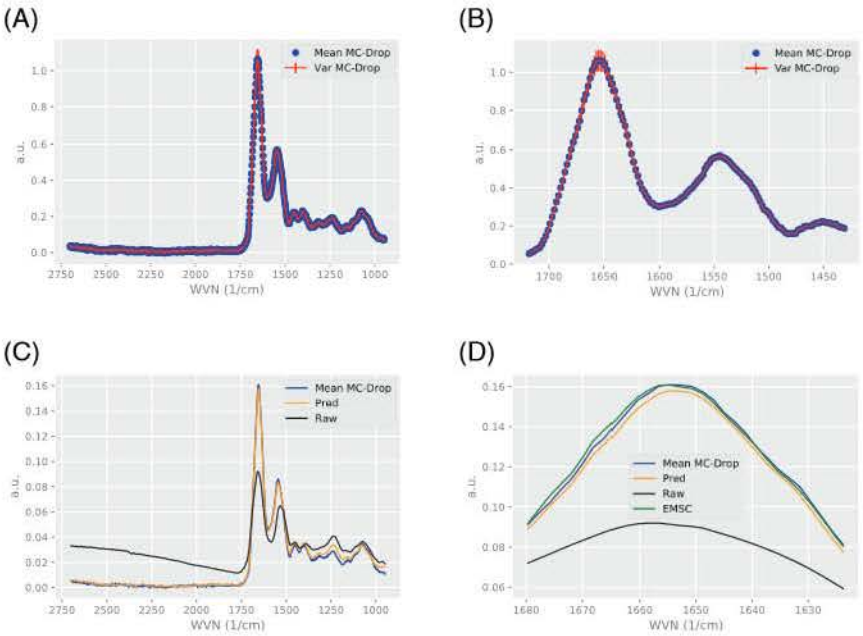

FIGURE 4 Panel A, Mean spectrum obtained by neural network S_0 including confidence interval obtained by MC dropout; B, Same as A, focusing on the amide bands of the spectrum and demonstrating the relatively low confidence in the regression around the amide I peak; Panel C, Comparison of mean spectra; Panel D, Same as C, focusing on the amide bands of the spectrum

deep neural networks, while all computations, in particular applying the trained neural networks, were performed on conventional CPU-based hardware only.

3.2 | Implementation

We utilized two implementations of the RMieS correction provided by the authors of[14]. Henceforth, we will refer to these implementations as *EMSC V2* and *EMSC V5*, respectively. The network S_0 was trained using raw spectra as input and *EMSC V2* corrected spectra as target output for regression learning. The *EMSC V5* implementation was used as a reference. All neural networks were implemented using the Theano framework, as described in Reference 18.

4 | RESULTS

4.1 | Downstream validation

Figure 2 panels **A**–**C** shows the comparison of the validation dataset for the FFPE data using the random forest introduced in Reference 1 as downstream classifier that classifies RMieS corrected spectra into one out of 19 different tissue components. Compared to the ground truth segmentation obtained from $C(R(x))$ for each pixel spectrum x, the approximation based classification constituted by $C(S_0(x))$ achieves an accuracy of 78% across all pixels in the whole-slide image displayed in panels E and F in Figure 2.

4.2 | Running time

To assess running times, we performed correction of a validation dataset of size 600×600 spectra. The time that has been recorded was averaged over 10 different runs each and are summarized in the Table 1.

4.3 | Characterization of approximation capabilities

As indicated in Figure 3, the corrected spectra obtained from network S_0 approximate the RMieS correction function with only little error. However, the deviation around the amide I peak around 1650 cm^{-1} is remarkably high. In fact, detailed inspection (Figure 3) indicates a band shift between the RMieS corrected ground truth spectrum and the neural network approximation, indicating a possibly unreliable approximation around the amide I region. To further assess this band shift, we performed Bayesian dropout validation, which yields a confidence interval at each wavenumber, as displayed in Figure 4. The confidence intervals are strikingly large around the amide I peak and coincide with an observed band shift between the neural network approximation and the RMieS corrected ground truth. Another explanation for this shift can be the transflection measurements used here which suffer from an electric field standing wave effect. It is known that this interference effect leads to a shift in the ratio of absorption bands.[8,10,22,37] Perhaps the network approximates this effect too in difference to the

RMieS. Unfortunately, this cannot be clarified based on the analyzed datasets within this work.

5 | DISCUSSION AND CONCLUSION

Our results clearly demonstrate that the RMieS correction for infrared spectra can be approximated by a neural network that produces practically useful corrected spectra, while using only a fraction of the computation time. Beyond the immediate and practically highly relevant benefit in terms of computational speedup, our results also contribute to the understanding and interpreting of what deep neural network models have learned during supervised training. In fact, in Reference 18, it was hypothesized that autoencoder-based pretraining for a *classifying* neural network may have learned to disentangle raw infrared pixel spectra in a manner such that the variance due to resonant Mie scattering has been separated from the variance that is due to vibrations at the molecular level. The fact that the same pretrained stacked autoencoder allows to compute corrected spectra adds further support to this hypothesis.

In general, it is important to keep in mind the inherent limitations of approximations obtained from deep neural networks as the one we have introduced here. In fact, the network function S_θ we obtain is a very local approximation of the RMieS correction function R in the sense that it works primarily for input spectra that sufficiently resemble the training data. In other words, as long as a raw spectrum x is obtained from FFPE samples of colon tissue, applied to similar substrate and spectroscopically measured in a similar manner, then $S_\theta(x)$ will produce spectra that will reliably resemble $R(x)$, with the restriction that only a special scattering was considered here. For a more comprehensive view of all optical effects, a correction of the data based on Maxwell's equations must be used, which has, to the authors' best knowledge, not been applied in case of large FTIR imaging datasets so far. It is a highly relevant question for future research to train networks that work reliably on a broader set of inputs, e.g. across tissue from different organs and being either FFPE or fresh-frozen as well as potentially being prepared on different substrate material, and optical corrections.

An important question arising from our work and the recent related approach from Magnussen et al.[20] is the choice of the network topology and the approach to train procedures. While beyond the scope of the present contribution, we believe that the three different validation approaches presented here will be helpful for a systematic comparison between the two procedures. Such comparison may also shed light on the disentanglement hypothesis emerging from Reference 18: Does the latent space of the different types of autoencoders separate essential features of FTIR in spectra, and, specifically, can we identify a clear separation between scattering and absorbance components in the latent space? An answer to this question is beyond theoretical interest, since it facilitates the interpretation and characterization of what features a deep neural network has learned during training. Such understanding will greatly contribute to understanding the strengths and also the limitations of deep neural networks for infrared spectroscopy in biomedical applications. An improved understanding of physical effects in latent space will finally also help improve approaches based on convolutional neural networks[38–40] that also take into account spatial information by classifying or segmenting whole images or image patches.

A natural and important question arising from neural network based approximations of physical models is how reliable the approximations are. To address this, we have contributed a Bayesian approach where we could show that the confidence obtained from the Bayesian network coincides with deviations between physical model and neural network based approximation. In our present case, the observed uncertainty in the amide I region supports two opposite hypotheses: On the one hand, uncertainty may result from a weak approximation capability of the neural network. On the other hand, the uncertainty may be inherent to the underlying physical model. While beyond the scope of our present contribution to resolve which hypothesis holds, the Bayesian approaches we introduce provide systematic means to not just interpret the reliability of neural network approximations, but potentially also uncertainties resulting from the approximated physical model itself. While we cannot fully resolve which of the two hypotheses holds, Bayesian estimates of uncertainty are a useful way to inspect deep learning models and are potentially useful in many applications of deep learning in vibrational spectroscopy. The dropout-based approach by Gal[29] is particular attractive since it is relatively easy to implement and has relatively modest demands in terms of computation time.

Even with the limited generalization guarantee resulting from relatively limited training data, the com-

highly relevant question for future research to train networks that work reliably on a broader set of inputs, e.g. across tissue from different organs and being either FFPE or fresh-frozen as well as potentially being prepared on different substrate material, and optical corrections.

An important question arising from our work and the recent related approach from Magnussen et al.[20] is the choice of the network topology and the approach to train the network. It is currently an open question whether the convolutional neural networks from References 19 and 20 or the pre-trained fully connected multi-layer perceptrons introduced here are more favorable for approximating the (different types of) EMSC correction

mates of uncertainty are a useful way to inspect deep learning models and are potentially useful in many applications of deep learning in vibrational spectroscopy. The dropout-based approach by Gal[29] is particular attractive since it is relatively easy to implement and has relatively modest demands in terms of computation time.

Even with the limited generalization guarantee resulting from relatively limited training data, the computational speedup constitutes a factor that makes our results promising from a practical perspective, since the high demand of computation time can easily become a road block in many practical settings, when e.g. dealing with whole slide images.

ACKNOWLEDGMENTS

This research was funded in part by the German Research Foundation (DFG MO 2804/1-1). Open Access funding enabled and organized by ProjektDEAL

DATA AVAILABILITY STATEMENT

Data and Software are available upon request from the authors. Software will be made puclicly avaialable in a forthcoming release of the OpenVibSpec open source software package.

ORCID

Axel Mosig https://orcid.org/0000-0001-7266-8323

REFERENCES

[1] C. Kuepper, F. Großerueschkamp, A. Kallenbach-Thieltges, A. Mosig, A. Tannapfel, K. Gerwert, *Faraday Discuss.* **2016**, *187*, 105.
[2] A. Kallenbach-Thieltges, F. Großerüschkamp, A. Mosig, M. Diem, A. Tannapfel, K. Gerwert, *J. Biophotonics* **2013**, *6*(1), 88.
[3] B. Bird, M. Miljković, S. Remiszewski, A. Akalin, M. Kon, M. Diem, *Lab. Invest.* **2012**, *92*(9), 1358.
[4] F. Großerueschkamp, A. Kallenbach-Thieltges, T. Behrens, T. Brüning, M. Altmayer, G. Stamatis, D. Theegarten, K. Gerwert, *Analyst* **2015**, *140*(7), 2114.
[5] P. Bassan, P. Gardner, *Biomedical Applications of Synchrotron Infrared Microspectroscopy,* The Royal Society of Chemistry, Cambridge **2010**, p. 260.
[6] T. G. Mayerhöfer, J. Popp, *Appl. Spectrosc.* **2020**, *74*(10), 1287.
[7] B. Mohlenhoff, M. Romeo, M. Diem, B. R. Wood, *Biophys. J.* **2005**, *88*(5), 3635.
[8] M. Miljković, B. Bird, M. Diem, *Analyst* **2012**, *137*(17), 3954.
[9] B. Zimmerman, V. Tafintseva, M. Bagcoglu, M. Høegh Berdahl, A. Kohler, *Anal. Chem.* **2016**, *88*(1), 803.
[10] T. G. Mayerhöfer, J. Popp, *Spectrochim. Acta A Mol. Biomol. Spectrosc.* **2018**, *191*, 283.
[11] P. Bassan, H. J. Byrne, F. Bonnier, J. Lee, P. Dumas, P. Gardner, *Analyst* **2009**, *134*, 1586.
[12] A. Kohler, J. Sule-Suso, G. D. Sockalingum, M. Tobin, F. Bahrami, Y. Yang, J. Pijanka, P. Dumas, M. Cotte, D. G. Van Pittius, et al., *Appl. Spectrosc.* **2008**, *62*(3), 259.
[13] H. Martens, E. Stark, *J. Pharm. Biomed. Anal.* **1991**, *9*(8), 625.
[14] P. Bassan, A. Kohler, H. Martens, J. Lee, H. J. Byrne, P. Dumas, E. Gazi, M. Brown, N. Clarke, P. Gardner, *Analyst* **2010**, *135*(2), 268.
[15] J. H. Solheim, E. Gunko, D. Petersen, F. Großerüschkamp, K. Gerwert, A. Kohler, *J. Biophotonics* **2019**, *12*(8), e201800415.
[16] K. E. Witzke, F. Großerueschkamp, H. Jütte, M. Horn, F. Roghmann, N. von Landenberg, T. Bracht, A. Kallenbach-Thieltges, H. Käfferlein, T. Brüning, K. Schork, M. Eisenacher, K. Marcus, J. Noldus, A. Tannapfel, B. Sitek, K. Gerwert, *Am. J. Pathol.* **2019**, *189*(3), 619.
[17] P. Pradhan, S. Guo, O. Ryabchykov, J. Popp, T. W. Bocklitz, *J. Biophotonics* **2020**, *13*(6), e201960186.
[18] A. P. Raulf, J. Butke, C. Küpper, F. Großerueschkamp, K. Gerwert, A. Mosig, *Bioinformatics* **2020**, *36*(1), 287.
[19] S. Guo, T. Mayerhöfer, S. Pahlow, U. Hübner, J. Popp, T. Bocklitz, *Analyst* **2020**, *145*(15), 5213.
[20] E. A. Magnussen, J. H. Solheim, U. Blazhko, V. Tafintseva, K. Tøndel, K. H. Liland, S. Dzurendova, V. Shapaval, C. Sandt, F. Borondics, et al., *J. Biophotonics* **2020**, Aug 25, e202000204.
[21] Olaf Ronneberger, Philipp Fischer, Thomas Brox, in International Conference on Medical Image Computing and Computer-Assisted Intervention, Springer, **2015**, pp. 234–241.
[22] T. G. Mayerhöfer, S. Pahlow, U. Hübner, J. Popp, *Analyst* **2018**, *143*(13), 3164.
[23] R. T. Graf, J. L. Koenig, H. Ishida, *Appl. Spectrosc.* **1985**, *39*(3), 405.
[24] Y. Bengio, A. Courville, P. Vincent, *IEEE Trans. Pattern Anal. Mach. Intell.* **2013**, *35*(8), 1798.
[25] Salah Rifai, Pascal Vincent, Xavier Muller, Xavier Glorot, Yoshua Bengio, Contractive Auto-Encoders: Explicit Invariance During Feature Extraction. **2011**.
[26] J. Denker, Y. LeCun, *Adv. Neural Inform. Process. Syst.* **1990**, *3*, 853.
[27] J. C. David, *Neural Comput.* **1992**, *4*(3), 448.
[28] N. Srivastava, G. Hinton, A. Krizhevsky, I. Sutskever, R. Salakhutdinov, *J. Mach. Learning Res.* **2014**, *15*(1), 1929.
[29] Yarin Gal, Zoubin Ghahramani, in International Conference on Machine Learning, **2016**, pp. 1050–1059.
[30] M. Weigert, U. Schmidt, T. Boothe, A. Müller, A. Dibrov, A. Jain, B. Wilhelm, D. Schmidt, C. Broaddus, S. Culley, M. Rocha-Martins, F. Segovia-Miranda, C. Norden, R. Henriques, M. Zerial, M. Solimena, J. Rink, P. Tomancak, L. Royer, F. Jug, E. W. Myers, *Nat. Methods* **2018**, *15*(12), 1090.
[31] H. Wang, Y. Rivenson, Y. Jin, Z. Wei, R. Gao, H. Günaydn, L. A. Bentolila, C. Kural, A. Ozcan, *Nat. Methods* **2019**, *16*(1), 103.
[32] C. Ounkomol, S. Seshamani, M. M. Maleckar, F. Collman, G. R. Johnson, *Nat. Methods* **2018**, *15*(11), 917.
[33] E. Moen, D. Bannon, T. Kudo, W. Graf, M. Covert, D. Van Valen, *Nat. Methods* **2019**, *16*, 1.
[34] C. L. Srinidhi, O. Ciga, A. L. Martel, *Med. Image Anal.* **2020**, *67*, 101813.
[35] P. Bassan, A. Kohler, H. Martens, J. Lee, E. Jackson, N. Lockyer, P. Dumas, M. Brown, N. Clarke, P. Gardner, *J. Biophotonics* **2010**, *3*(8–9), 609.
[36] G. E. Hinton, R. R. Salakhutdinov, *Science* **2006**, *313*(5786), 504.
[37] P. Bassan, J. Lee, A. Sachdeva, J. Pissardini, K. M. Dorling, J. S. Fletcher, A. Henderson, P. Gardner, *Analyst* **2013**, *138*(1), 144.
[38] D. Schuhmacher, K. Gerwert, A. Mosig, *medRxiv* **2020**. https://doi.org/10.1101/2020.02.27.20028845.
[39] A. Signoroni, M. Savardi, A. Baronio, S. Benini, *J. Imaging* **2019**, *5*(5), 52.
[40] S. F. El-Mashtoly, D. Niedieker, D. Petersen, S. D. Krauss, E. Freier, A. Maghnouj, A. Mosig, S. Hahn, C. Kötting, K. Gerwert, *Biophys. J.* **2014**, *106*(9), 1910.

How to cite this article: Raulf AP, Butke J, Menzen L, et al. A representation learning approach for recovering scatter-corrected spectra from Fourier-transform infrared spectra of tissue samples. *J. Biophotonics*. 2021;14:e202000385. https://doi.org/10.1002/jbio.202000385